ADVANCED INTELLIGENT SYSTEMS
Open Access
www.advintellsyst.com

Tendon-Driven Compliant Wheel-Less Snake Robot for Undulatory Locomotion Using Conformable Ground Contacts

*Serdar Incekara, Seongil Kwon, Gangil Kwon, and Junhyoung Ha**

Replicating the flexible and efficient locomotion of biological snakes remains a significant challenge in robotics. Conventional snake robots, often built from serially linked rigid joints, require complex control strategies to simultaneously manage body undulation and propulsive ground forces. Based on the previous theoretical study, this article presents the first physical realization of a new principle that simplifies locomotion control by decoupling these two tasks. The core idea is that by using a flexible continuum body, different gaits can be generated by superimposing simple globally-applied tensions (for vertical bending and axial twisting) onto a basic planar undulation. These global tensions, combined with the robot's compliance and weight, passively shape the required ground contact patterns, eliminating the need for active force control at individual points. The design and implementation of a tendon-driven continuum snake robot that embodies this principle is presented. The robot uses globally routed tendons, actuated by centrally-located motors, to create uniform bending and twisting. Through experiments, it is demonstrated that the robot can produce three distinct gaits—forward, backward, and sidewinding—on flat ground simply by changing the global actuation mode, and demonstrate its capability for intuitive steering.

1. Introduction

Snake robots have been a subject of research for several decades, driven by the desire to replicate the unique and efficient locomotion of biological snakes. The fascination with these robots stems from their potential applications in search and rescue missions, reconnaissance and exploration tasks, and industrial inspections, where their slender and flexible bodies can navigate through confined and complex environments that are inaccessible to conventional robots.

Despite decades of research, however, replicating the fluid locomotion of biological snakes remains a difficult challenge, especially on flat ground where there are no external features to push against. Early solutions often involved wheels to create directional friction anisotropy[1–5] or used obstacle-aided locomotion strategies that rely on the environment to generate thrust.[6–9] While effective in certain scenarios, these methods limit a robot's versatility and do not capture the fundamental principles of a biological snake's locomotion on open surfaces.

The dominant approach in wheel-less snake robotics has involved linking rigid sections with motors at each joint.[10–12] These robots have demonstrated impressive capabilities, including climbing and sidewinding.[12,13] However, their reliance on hyper-redundant rigid joints poses a significant control complexity: to generate propulsion, these robots require high-dimensional control over each joint to coordinate both the body shape and the ground contact forces. The simultaneous management of the body wave and the resulting ground forces remains a primary challenge.

This article explores an alternative approach using tendon-driven continuum robots, which offers a different philosophy for locomotion. A continuous backbone more closely resembles the flexible spine and distributed muscles of a biological snake. This inherent compliance provides benefits for passively adapting to terrain and interacting more safely with the environment.[14–16] In our previous theoretical study,[17] we introduced a locomotion principle that uses this compliance to greatly simplify control. We demonstrated theoretically that the complex relationship

S. Incekara
Advanced Materials and Systems Research Division
Korea Institute of Science and Technology (KIST)
Seoul 02792, South Korea

The ORCID identification number(s) for the author(s) of this article can be found under https://doi.org/10.1002/aisy.202501183.

DOI: 10.1002/aisy.202501183

S. Kwon
Advanced Research Team
Endorobotics Co., Ltd.
Seoul 03082, South Korea

G. Kwon
Department of FAB Engineering and Operations
Samsung Electronics
Suwon 16677, South Korea

J. Ha
Department of Mechanical Engineering
Ulsan National Institute of Science and Technology (UNIST)
Ulsan 44919, South Korea
E-mail: j.ha@unist.ac.kr

between body shape and ground forces could be decoupled: that lengthwise-globally applied vertical bending and axial twist can be translated into the ground contact distributions required for various undulatory gaits. This article presents the design, fabrication, and experimental validation of the first robotic platform to implement this principle. While the present study focuses on flat ground locomotion, the compliant architecture was chosen deliberately, as its ability to passively conform to uneven surfaces is a key advantage for our future work in complex 3D environments.

The main contribution of this aticle is the physical implementation and experimental validation of this novel locomotion principle. The strategy relies on combining two distinct actuation modes: 1) segment-wise local actuation to generate a continuous planar undulation, and 2) lengthwise-global actuation of body tensions to control vertical bending and axial twisting. This global actuation uses the robot's passive compliance and its own weight to shape the desired ground contact patterns, such as the sinus-lifting body shape for forward motion, without needing to explicitly model or control forces along the body. This approach shifts the complexity of force management from the controller to the physical dynamics of the robot itself, which aligns with a key design principle of embodied intelligence.[18]

We remark that our global-tension actuation is among possible engineering solutions to replicate the ground contact patterns seen in biological snakes; it remains unknown if their neuromuscular systems have similar functionalities. Instead of investigating the biological mechanisms, this study focuses on building a proof-of-concept implementation extending our previous theoretical work[17] and reproducing various gaits observed in biological snakes.

In this article, we present the design, development, and validation of a tendon-driven compliant snake robot that is the first physical implementation of this global actuation principle. The main contributions are: 1) The design of a continuum snake robot with a novel global actuation mechanism, with justifications for key design choices, such as the number of modules and the central placement of actuation motors to mitigate tendon-path frictional losses. 2) The demonstration that three fundamental snake gaits (forward undulation, backward undulation, and sidewinding) can be generated from a single planar wave pattern simply by changing the applied global tension, thus validating our previously proposed theory. 3) Experimental validation of these gaits on a flat indoor surface, including performance measurements and a demonstration of intuitive, continuous steering for navigation.

The remainder of this article is organized as follows: Section 2 reviews related works, providing a comprehensive overview of previous research and developments in the field of snake robots. Section 3 outlines the methodology, including the hardware structure and control scheme for snake locomotion. Section 4 details the component designs, the actuation method, and the mechatronics system for robot teleoperation. Section 5 describes the joint and motor control method, and Section 6 presents the experimental results, followed by the conclusion in Section 7.

2. Related Works

Snake robots have been extensively studied to develop various mechanisms and control schemes. This section reviews key developments in both rigid and soft snake robots, as well as advances in locomotion control.

2.1. Rigid Snake Robots

Rigid snake robots can be categorized into wheeled and wheel-less types, as reviewed below.

2.1.1. Wheeled Snake Robots

Biological snakes utilize anisotropic skin properties to facilitate forward thrust, with minimal skin friction in the forward direction and greater friction in the backward and sideways directions.[19] Wheels have been used in snake robots to replicate this frictional anisotropy. Passive wheels were incorporated in various designs,[1–3,20,21] whereas active wheels were employed to provide greater control.[4,5]

2.1.2. Wheel-Less Snake Robots

Wheel-less snake robots were developed to overcome the typical limitation of wheeled robots, which is their restricted ability to navigate various terrains. These robots require more sophisticated control and planning, utilizing environmental contacts. One class of motion control for these robots is obstacle-aided control, where robots push or pull against surrounding objects to propel themselves.[6–9,22]

Some robots have demonstrated motion in more complex environments. For example, the Carnegie Mellon University (CMU) modular snake robot and other similar robots have exhibited rod-climbing motion.[12,23,24] Additionally, a robot capable of climbing a ladder was presented in.[25] The study in[26] introduced a nonsliding gait to navigate through virtually defined hoops. Snake locomotion inside pipes was also studied in.[12,27,28]

2.2. Soft Robots

Soft snake robots utilize compliant materials and structures to achieve flexible and adaptive locomotion. These robots can deform their bodies to conform to various obstacles, providing a distinct advantage over rigid designs. A soft snake robot with passive wheels that exhibits pressure-operated undulation was developed in.[14] A novel soft actuator for undulatory locomotion and its gait patterns were presented in.[15] Pneumatic-actuated soft robots demonstrating kirigami skin-aided lateral undulation and rod-climbing motion were presented in,[16,29] respectively. Sidewinding motions of soft snake robots were demonstrated in.[30,31]

2.3. Locomotion Control

Our review of locomotion control in snake robots focuses on wheel-less robots, which are more relevant to our study.

2.3.1. Obstacle-Aided Control

Many previous works on snake robot locomotion have focused on utilizing environmental objects to propel the robots. This

approach is inspired by the behavior of biological snakes, which often use objects in their environment to push off and navigate through complex terrains. Obstacle-aided control mainly relies on lateral supports from objects to restrict sideways slip and only allow forward sliding.[6–9] These lateral supports provided by obstacles offer a similar advantage to using passive wheels, facilitating forward movement with minimal sideways slip.

2.3.2. Undulatory Locomotion

Biological snakes exhibit various types of undulatory locomotion, including sinus-lifting forward locomotion,[19] center-lifting backward locomotion,[32] and sidewinding.[13,33] These motions are based on similar body undulation, with different ground contacts between the motions causing different directional thrusts.

Sidewinding is the most commonly implemented locomotion mode in snake robots.[13,30,31,33,34] This is because sidewinding utilizes static ground contacts sequentially made over undulation cycles, which is fundamentally not different from legged locomotion. The physics of this locomotion mode is easier to understand and implement in robots.

Center-lifting backward locomotion is observed only in very limited snake species, such as Cerastes vipera, and typically under experimental stimulation conditions.[32] In these cases, the animals exhibit alternating lateral bending while lifting the central portion of the body, producing a net backward displacement. While this behavior is not a common natural gait, the resulting ground-contact pattern—contacts occurring at the lateral edges of body curves—provides valuable insight into the mechanics of thrust generation.

In this motion, snakes make ground contacts at the leftmost and right-most edges of the body curve. A similar motion principle can be found in pipe-navigating snake robots.[12,27,28] When these robots fit tightly in a pipe and undulate, they naturally make contact with the pipe at the side edges of their body curve.

In our work, we use the term backward locomotion to denote the robotic realization of this center-lifting contact pattern rather than an attempt to reproduce typical biological backward crawling. The correspondence is therefore conceptual: the same body-contact configuration is exploited to achieve reverse propulsion in a controlled robotic setting.

2.3.3. Nonundulatory Snake Locomotion

In addition to undulatory locomotion, biological snakes are capable of rectilinear and concertina locomotion, which involve distinct contact and actuation strategies. Rectilinear locomotion produces slow, linear advancement by sequentially lifting and pulling the ventral scales, whereas concertina motion relies on alternating anchoring and extension phases of the body to progress within confined spaces. These principles have also inspired implementations in both rigid and soft snake robots.[35–37] Although these modes are not utilized in this study, they are included here for completeness to provide a broader context of snake-robot locomotion.

2.3.4. Mode-Switching Control

Several studies have explored gait-transition strategies in modular or joint-actuated snake robots, primarily through control algorithms rather than mechanical reconfiguration. Central pattern generator (CPG)-based frameworks have been particularly effective for generating rhythmic locomotion and enabling smooth transitions between different gait patterns.[37,38] Although our present method achieves mode switching through global tendon actuation instead of CPG-based control, these works highlight complementary strategies toward achieving versatile and adaptive multi-gait snake locomotion.

2.3.5. Passive Ground Contacts in Snake Locomotion

Although sinus-lifting forward locomotion is the most representative snake locomotion, it has rarely been demonstrated in snake robots. This motion relies on continuous sliding contacts that generate propulsion through friction, which are difficult to model and actively control in conventional rigid-link robots. To the best of our knowledge, our previous study[17] presented the first demonstration of sinus-lifting forward locomotion, as well as center-lifting backward locomotion and sidewinding, using a single wheel-less robotic platform without relying on obstacle interactions.

The key insight of that work was a locomotion principle that leverages the robot's own body compliance and weight to *passively* form the necessary ground contact patterns. Instead of explicitly controlling contact forces at each joint, the control is simplified by decoupling the generation of the body wave from the generation of ground contacts. The principle states that distinct gaits can be produced by combining a globally-applied body tension with a planar undulation. The compliant body then deflects under gravity to shape the required ground contact profile. The core locomotion principle will be described in detail in the following section.

3. Method

In this section, we first review the underlying principles of snake locomotion as discovered in our previous work,[17] followed by an overview of our hardware implementation to realize these locomotion principles in a robotic snake mechanism.

3.1. Locomotion Principle

Our previous study on snake locomotion revealed that body compliance and lengthwise-globally applied vertical bending and axial twisting can enable natural snake movement in snake robots.[17] Specifically, as illustrated in **Figure 1**, the following principles can be used to achieve undulatory snake locomotion: 1) **Upward vertical bending**, applied globally, during planar undulation produces sinus-lifting forward locomotion. 2) **Downward vertical bending**, applied globally, during planar undulation produces center-lifting backward locomotion. 3) **Axial twisting**, applied globally, during planar undulation produces sidewinding.

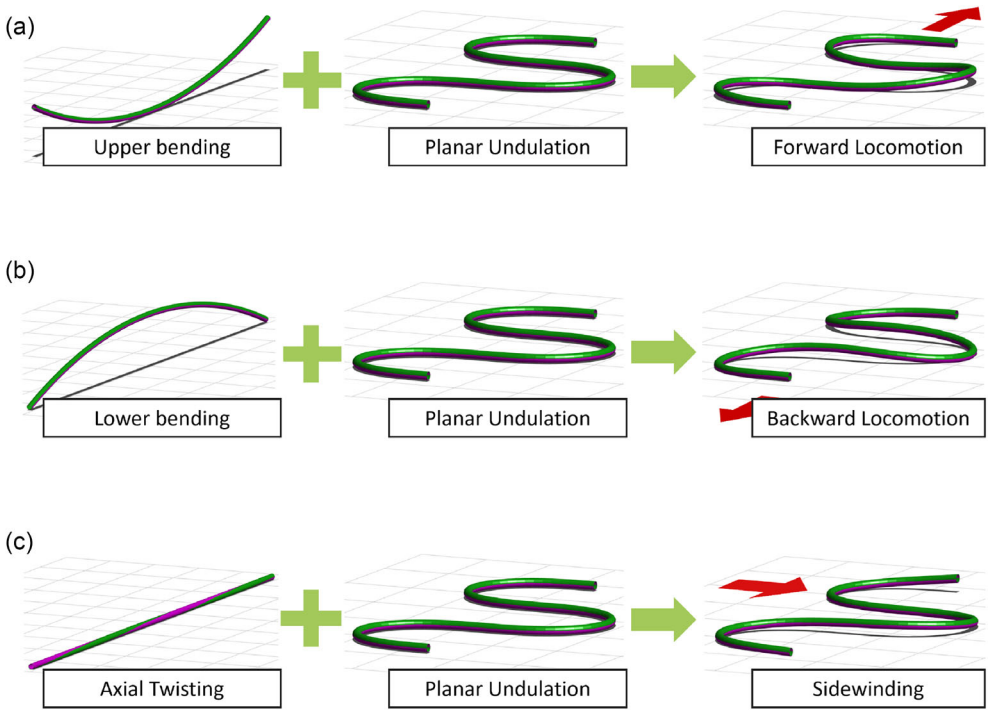

Figure 1. Undulatory locomotion principles using lengthwise-globally applied body tensions: a) forward locomotion, b) backward locomotion, and c) sidewinding. The red arrows represent the locomotion directions, and the body is bi-colored to visualize the body twist. Adapted with permission.[17] Copyright 2017.

3.2. Implementation Overview

To apply our locomotion principles described in Section 3.1, the robot hardware must be capable of adaptively controlling vertical bending and axial twisting during motion. This poses a significant challenge to the design of the robot mechanism. Herein, we overview how we have implemented these actions in our tendon-driven snake robot mechanism. More details on the module and joint design, as well as the mechatronics system, are provided in the following section.

3.2.1. Hardware Configuration

Our robot is composed of 13 modules in series, each module equipped with a servo motor. We utilized ten single-axis and three dual-axis servo motors, with five single-axis motors at the front and five at the rear, and the three dual-axis motors in the middle, as depicted in **Figure 2**. Continuum joints are implemented between the motors, each comprising a spring and a central backbone, to provide compliance to the robot. Tendons are used to bend the continuum joints driven by adjacent motors. The overall weight and length were 2.21 kg and 1.25 m, respectively.

The choice of 13 modules, forming 12 joints, providing sufficient contact point distribution along the robot's length, enabling efficient propulsion when suitable motion parameters are applied. Moreover, this configuration achieves a good resolution for shaping smooth snake-like curves. Additionally, the divisibility of 12 by 2, 3, and 4 allows for flexible curvatures and diverse

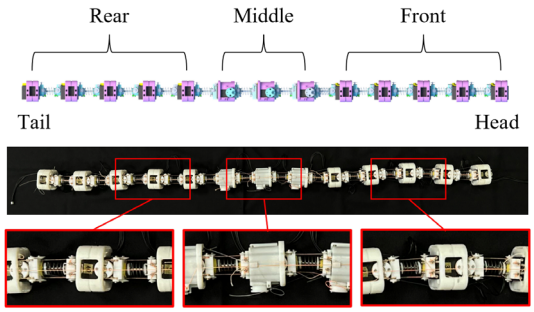

Figure 2. Our snake robot mechanism consists of 13 motors arranged in series, with the three central motors being dual-axis. These dual-axis motors utilize their second axes for vertical bending and axial twisting.

contact patterns along the body, enabling to implement the motions effectively.

The two key elements in implementing our locomotion principles are planar undulation and vertical bending/axial twisting actuation. For planar undulation, the 12 continuum joints alternate bending left and right at different phases between motors, producing a propagation of flexural waves along the robot's length. Additionally, vertical bending and axial twisting are actuated by the second axes of the dual-axis motors: the first axes are used for planar undulation, while the second axes are connected to additional tendons routed globally through the robot's body–straight paths along the back (top surface) and abdomen (bottom surface) and spiral paths around the body. This configuration allows for lateral bending of the continuum joints to create

undulation, with globally routed tendons controlling ground contacts during the movement.

3.2.2. Global Bending and Twisting Actuation

This section demonstrates how global bending and twisting actuations produce the ground contact patterns essential for desired locomotion. As outlined in Section 3.1, our locomotion principle relies on applying global vertical bending and axial twisting to a compliant body, which then passively forms the desired ground contacts. This mechanism is critical for generating the necessary propulsive forces without active control. We now show how our robot's physical configuration achieves these theoretically-derived contact patterns, forming the foundation for forward, backward, and sidewinding locomotion.

Forward Locomotion (Figure 3): Global upward bending is applied by tensioning the tendons routed along the robot's dorsal side. **Figure 3**a illustrates the theoretical contact force distribution under this tension,[17] which aligns with observations of forward locomotion in biological snakes.[19] Figure 3b shows the physical configuration of the robot, with the smaller images highlighting its body lifts. This actuation is intended to generate forward locomotion, as inferred from the resulting configuration that resembles the body curvature of biological snakes in their sinus-lifting forward motion.

Backward Locomotion (Figure 4): Conversely, pulling the tendons routed along the robot's abdomen creates a global downward bend. **Figure 4**a shows the theoretical contact force distribution given this tension,[17] and Figure 4b presents the corresponding physical posture of the robot, with the insets showing its body lifts. This configuration produces backward locomotion, as observed in the center-lifting motion of Cerastes vipera.[32] In contrast to the previous case, the robot makes ground contact at the leftmost and rightmost edges of its body, while the central sections are elevated.

Sidewinding (Figure 5): Finally, tensioning the spirally routed tendons induces a global axial twist along the robot's body. The theoretical contact distribution under this torsion is depicted in **Figure 5**a,[17] where sections of the body between the leftmost and rightmost edges are alternately in and out of contact with the ground. Figure 5b shows the corresponding physical posture of the robot, with the insets showing its body lifts. This ground contact pattern resembles that of biological snakes during sidewinding, as reported in.[13,33]

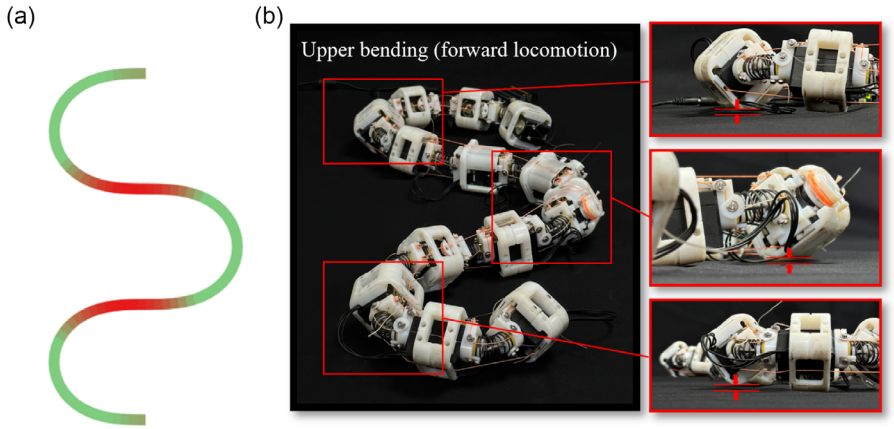

Figure 3. Passive generation of the sinus-lifting posture for forward locomotion through global upward bending: a) Theoretical ground contact force distribution (red indicates higher force). b) Robot's corresponding physical posture with annotated body lifts.

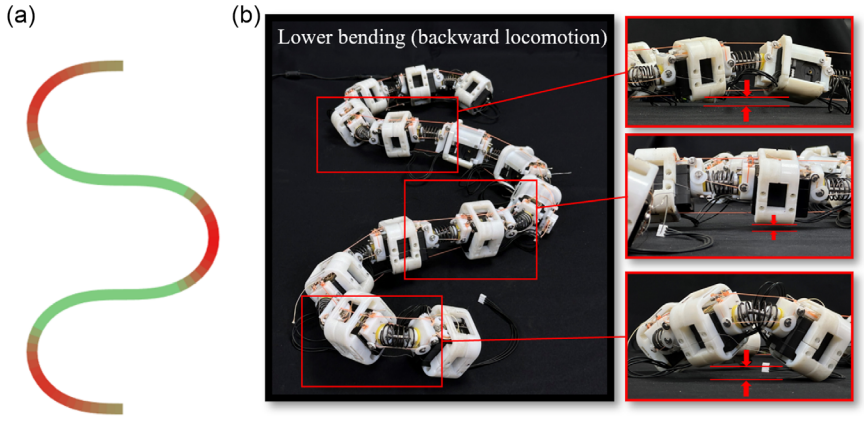

Figure 4. Passive generation of the center-lifting posture for backward locomotion through global downward bending: a) Theoretical ground contact force distribution (red indicates higher force). b) Robot's corresponding physical posture with annotated body lifts.

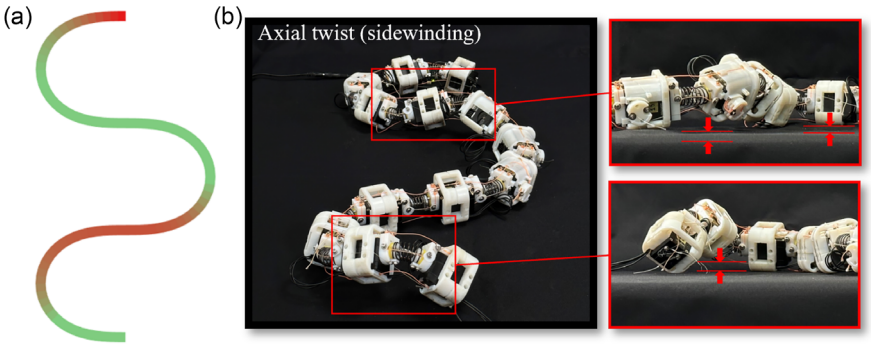

Figure 5. Passive generation of contact pattern for sidewinding through global axial twisting: a) Theoretical ground contact force distribution (red indicates higher force). b) Robot's corresponding physical posture with annotated body lifts.

4. Hardware Development Details

This section presents more detailed descriptions of the hardware development and mechatronics system, including the continuum joint with its actuation method, the module design, the global bending and twisting actuation, and the overall mechatronics system for robot teleoperation.

4.1. Continuum Joint

Our locomotion principles in[17] rely on the robot's natural deflection caused by the robot's body compliance, not only in bending but also in torsion. To provide compliance to the robot, we developed continuum joints to connect between modules, each of which was built with a coil spring and a central backbone, as illustrated in **Figure 6**.

The coil springs possess a restorative force that allows them to smoothly bend in response to external forces and return to their original position when the external force is released, which gives bending compliance to the robot mechanism. To assemble the springs with the adjacent modules, 3D printed adapters were attached to the motors, and the springs were tightly fixed to the adapters (see Figure 6). The springs bend through tendons connected between consecutive modules, which will be described in more detail in the following subsection.

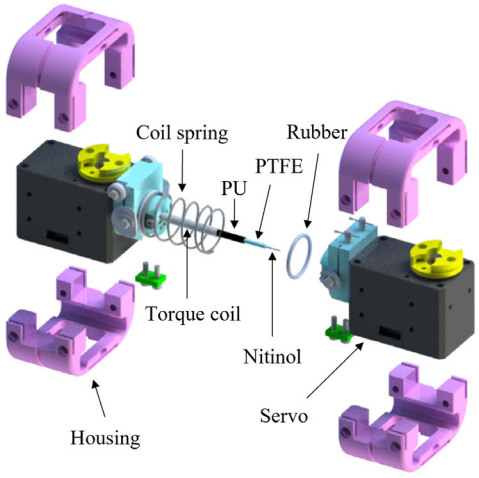

Figure 6. Components of our continuum joint and adjacent modules. The rubber is used to fill the gap between the coil spring and the adaptor.

While the tendon tensions cause bending in the springs, they can also lead to spring compression. This means that not all tension is used for pure bending, which reduces the bending amplitude of the joints during planar undulation. To minimize this bending loss, a central backbone was placed at the center of each spring, preventing spring compression while allowing for bending.

Although our locomotion principles require torsional compliance, high flexibility in torsion can cause unpredictable robot behaviors, such as tangling and rolling. While the coil spring is relatively stiffer in torsion than in bending compared to other solid structures (e.g., rods), we encountered issues when the springs were used alone for torsional resistance: the tension from multiple tendons during planar undulation could easily cause torsion, disrupting stable ground contact and leading to the robot flipping over. To mitigate this behavior, we included a torque coil in the central backbone of each joint. The torque coil exhibits flexible bending but excellent torque transmission, making it ideal for this application. Typically, it is made by winding two stainless steel wires in opposite spiral directions, resulting in low bending stiffness and high torsional stiffness. We used a torque coil manufactured by Asahi Intecc, with an inner diameter of 3 mm and an outer diameter of 3.9 mm. To prevent buckling, we filled the inside of the torque coil with a NiTi rod with a diameter of 0.8 mm, along with PTFE and PU tubes.

4.2. Joint Actuation Mechanism

The continuum joints are attached to consecutive motors using the 3D-printed adaptors. As depicted in **Figure 7**, two tendons are connected from the rotor of one motor to the adapter of the adjacent motor. As the motor rotates, one tendon is pulled while the other is released, causing the continuum joint to bend toward the pulled tendon. This bending motion produces the planar undulation of the robot.

The tendon routing is of great importance in the design of the actuation mechanism. In particular, it is crucial that the tendons run parallel to the central backbone of the joint on the same horizontal plane to ensure that the joints bend only in the left and right directions without tilting upwards or downwards. Since the

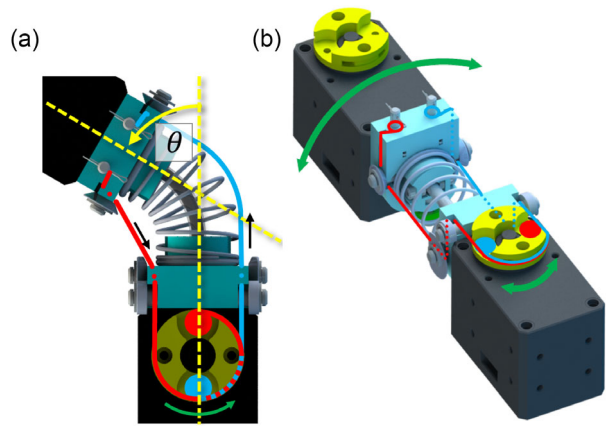

Figure 7. Joint actuation mechanism: a) Joint bending induced by tendon displacement. b) Tendon paths with multiple 90° turns.

ends of the tendons are located at the top of the motors, directly connecting the tendons in the shortest paths results in horizontal misalignments between the tendons and the backbone. To resolve this issue, slits were made in the adapters to allow the tendons to pass through. As shown in Figure 7b, the tendons run through multiple 90° turns via stainless steel pillars attached to the adapters. The surfaces of the pillars were confirmed to be smooth to minimize friction when the tendons slide over them. To prevent the tendons from deviating from their paths during motor rotation, circular guides are attached to both sides of each pillar.

4.3. Module Housing and Global Bending/Twisting Actuation

As illustrated in Figure 6, each module is wrapped with a 3D-printed plastic housing to provide the robot with enhanced durability and tendon paths for the global bending and twisting actuation. We fabricated the housing using VeroPureWhite (Stratasys Ltd., USA), known for its high strength and printing precision, making it suitable for our purpose.

The actuation mechanism for global bending and twisting involves tendons running through the entire length of the robot in straight and spiral paths, as depicted in **Figure 8**. A key aspect of this system is the use of dual-axis motors. The first axes of these motors are used for the planar bending actuation of the continuum joints. As shown in Figure 8b, the second axes are located on the side of the motors. We designed rotors for these axes, where the globally routed tendons are connected. The other ends of the tendons are fixed at the head and tail of the robot. By rotating the motors over multiple revolutions, the tendons wrap around the rotors, resulting in tendon tensions for vertical bending and axial twisting. These actions are taken differently in different locomotion types. For forward movement, the red tendons in Figure 8 are wound while the blue tendons are unwound,

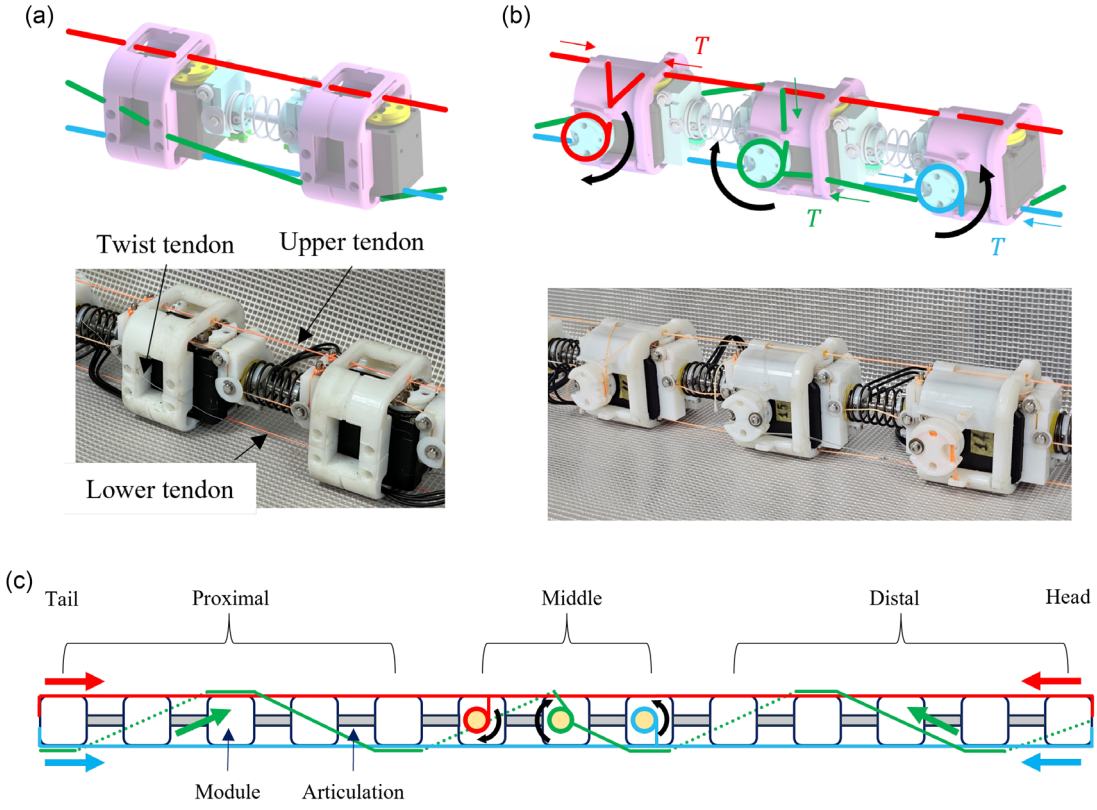

Figure 8. Diagrams and physical hardware images illustrating the paths of globally routed tendons: a) Tendon paths on modules with single-axis motors. b) Tendon paths on modules with dual-axis motors. c) Tendon paths over the entire robot length. The red tendons are responsible for the upper bending required for forward locomotion, while the blue tendons enable the lower bending needed for backward locomotion. Additionally, the green tendons are routed through the housings in spiral paths to create an axial twist for sidewinding.

whereas, in backward locomotion, the tendons are wound or unwound in the opposite way. In sidewinding, only the green cables are wound.

The dual-axis motors are placed in the middle of the robot (i.e., 6th, 7th, and 8th modules from either the head or the tail). Consequently, each second axis of the dual-axis motors is connected to two tendons, one going to the head and the other to the tail, resulting in a total of six body-spanning tendon paths originating from the center. This motor placement was determined based on our experimental results, which showed significant tension loss due to friction at the tail when the dual-axis motors were located at the head. By placing the motors in the middle, the tension losses are symmetrically distributed over the length of the robot.

Additionally, it is worth noting that the tendons used for joint bending are highly rigid in elongation, as compliance naturally comes from the joint structure. However, using rigid tendons for global bending and twisting caused issues with inflexible motion due to the tendon length constraints. To address this, we concatenated flexible urethane cables with rigid cables, attaching the flexible ends to the head and tail and the rigid ends to the motors. This combination provides greater compliance in vertical bending and axial twisting, enabling more fluent snake locomotion.

Regarding the combined cable configuration, two types of rigid cables were employed depending on the motion direction: braided fishing lines were used for the upper and lower tendons responsible for forward and backward bending, while steel cables were used for axial twisting in the sidewinding mode. Steel cables were selected for axial twisting due to their higher durability against frictional wear, since the helically routed tendons experience sharper bending angles within the housings. Each of these six tendons includes a flexible urethane segment, with varying portions of 10% to 20% of the total tendon length, which provides the necessary compliance for smooth deformation. To characterize the urethane material's elasticity, a tensile test was conducted using a handheld force gauge. When subjected to a 1 N load, the urethane cable elongated by 20.9% of its original length, indicating sufficient flexibility for global bending and twisting while maintaining stable tension transmission across the body.

While friction anisotropy is known to enhance locomotion efficiency in biological snakes, it is not a prerequisite for achieving the gaits demonstrated in this study. Our robot employs an isotropic ventral surface because the primary objective is to verify that distinct locomotion modes can emerge purely from ground-contact configuration and global actuation, as predicted in our previous theoretical work. Nevertheless, anisotropy can be optionally introduced by adding a skin or directional surface layer to improve traction and efficiency on certain terrains. The current results confirm that the proposed locomotion principle—achieving motion through controlled ground contacts—remains valid even without anisotropic surface design.

4.4. Mechatronics System for Actuation and Teleoperation

Potential issues with using multiple motors in series include complicated wiring for signal and power and the space occupied by motor drivers. To avoid these issues, we used Dynamixel motors, manufactured by ROBOTIS Inc., Korea, which are equipped with built-in drivers and support the TTL communication protocol. The TTL communication enables serial connection of the motors, which significantly simplifies power and signal wiring.

Specifically, for single-axis motors, the XH430-W350-T model was chosen, and for dual-axis motors, the 2XC430-W250-T model was selected. These motors can generate 3.4 Nm and 1.4 Nm of torque, respectively. Their dimensions (w × h × d) are 28.5 × 46.5 × 34 mm and 36 × 46.5 × 36 mm, and they weigh 82 g and 98 g, respectively.

The user interface includes a desktop application and a wireless joystick. To communicate with the motors, we used an Arduino MKR WiFi 1010 and its compatible Dynamixel Shield. The Arduino board reads motor values and sends commands to the motors through the Dynamixel Shield. The desktop application was developed to monitor the status of the motors and send motion parameters and joystick inputs to the Arduino board via Bluetooth Low Energy (BLE) (**Figure 9**).

5. Locomotion Control

To control the robot, we established a bending model for the continuum joints and implemented a motor position-control scheme to propagate flexural waves along the robot's length. Additionally, we provide a simple modification of the target angles in the motor control to achieve steerability for the robot.

5.1. Bending Model of Continuum Joint

The bending angle of our continuum joint is determined by the displacement of the pulling tendon. To establish the relationship between the motor angle and the joint's bending angle, we adopt the constant curvature assumption, as utilized in many other bending models of continuum mechanisms.[39]

Let $\alpha \in \mathbb{R}$ denote the motor angle and $\theta \in \mathbb{R}$ denote the joint's bending angle, as defined in Figure 7a. When the motor is rotated at a positive angle (i.e., counter-clockwise rotation), the left-side tendon is pulled by $r\alpha$, where $r \in \mathbb{R}$ is the radius of the motor's rotor. This situation is illustrated in **Figure 10**. Note that the bending angle θ is identical to the central angle of the backbone arc.

Let us define a set of length variables, a, d, l, x, y and R, as denoted in Figure 10. From the black triangle in Figure 10b, we obtain

$$R = (y + a)\cot\frac{\theta}{2} \tag{1}$$

$$y = x\tan\frac{\theta}{2} \tag{2}$$

where x is the radius of the backbone arc, i.e., $x = l/\theta$. By substituting this equation and (2) into (1), we can express R as

$$R = \frac{l}{\theta} + a\cot\frac{\theta}{2} \tag{3}$$

The length of the red line in Figure 10b is the retracted tendon length, which is $2a + l - r\alpha$. The isosceles triangle including the

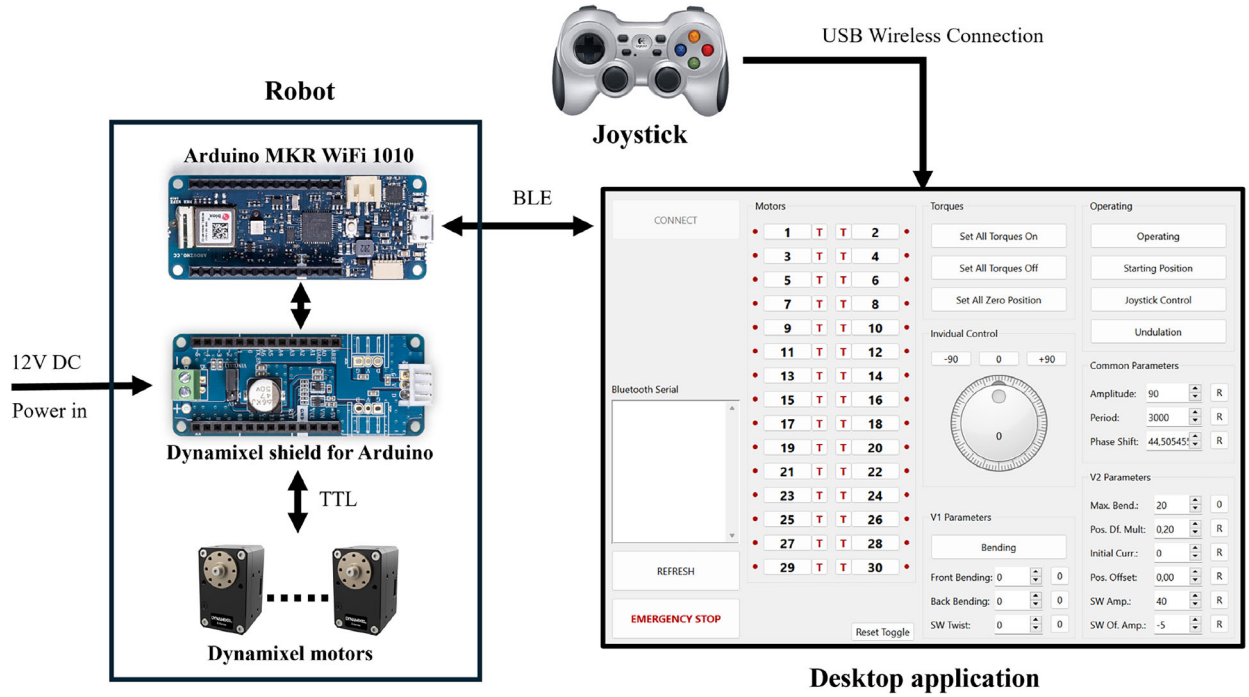

Figure 9. Overall mechatronics system to actuate and teleoperate the robot: An Arduino board is connected to the motors through a Dynamixel shield. A desktop application was developed to communicate with the Arduino board and a joystick.

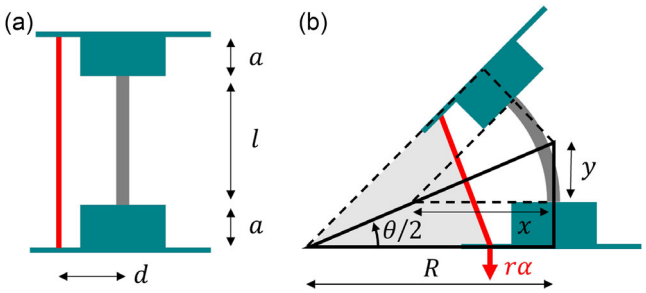

Figure 10. Bending geometry of continuum joints: a) before bending, and b) after bending. The values of a, d, l and r in our continuum joints are 7, 10.5, 20, and 10.5 mm, respectively. The red line represents the left-side tendon, while the right-side tendon is not visualized.

red line (i.e., the gray triangle in Figure 10b) can be divided in half into two right triangles, where we can derive

$$2a + l - r\alpha = 2(R - d)\sin\frac{\theta}{2} \tag{4}$$

Finally, substituting (3) into (4) yields the motor angle α expressed in terms of the bending angle θ

$$\alpha = \frac{2a}{r}\left(1 - \cos\frac{\theta}{2}\right) + \frac{l}{r}\left(1 - \frac{2}{\theta}\sin\frac{\theta}{2}\right) + \frac{2d}{r}\sin\frac{\theta}{2} \tag{5}$$

When the right-side tendon is pulled by a negative α, the above equation remains almost identical, with the signs of the first two terms on the right side being flipped.

Note that Equation (5) determines the motor angle α given a desired bending angle θ. When the bending angle is smaller than 180° (i.e., $0 < \theta < 180°$), the derivative of (5) with respect to θ is always positive. This means that α monotonically increases with increasing θ, indicating that smooth motor swings generate smooth joint swings without introducing any jittering.

5.2. Motor Control

The control of the snake robot is governed by the coordinated movement of its joints, which is crucial for achieving the desired locomotion patterns. In our robot, each motor connected to the joints is position-controlled by a sinusoidal function of time.

As the joints must bend to propagate waves through the robot length, the sinusoidal function contains two terms varying terms, including a time-dependent term and a motor position-dependent term, as similarly presented in[17]

$$\alpha_i(t) = \alpha_{\max}\sin(\phi_0(t) + \psi_i) \tag{6}$$

where $\alpha_i(t) \in \mathbb{R}$ represents the motion of the i-th motor, $t \in \mathbb{R}$ is the time variable, $\alpha_{\max} \in \mathbb{R}$ is the amplitude of motor swing, and $\phi_0(t) \in \mathbb{R}$ and $\psi_i \in \mathbb{R}$ are the time-dependent and motor position-dependent terms, respectively, defined as

$$\phi_0(t) = 360°\frac{t}{T} \tag{7}$$

$$\psi_i = -i\Delta\psi \tag{8}$$

Here $T \in \mathbb{R}$ is the period of undulation, i is the motor index, and $\Delta\psi$ is the phase shift between motors. Note that the

amplitude $\alpha_{\max}$ is computed using Equation (5) for the desired bending swing range.

5.3. Steering Control

Steering the direction of the robot's locomotion is an important functionality when the robot is teleoperated with a joystick. Implementing steerability in snake locomotion is not straightforward, particularly for sidewinding and backward locomotion. Meanwhile, forward locomotion can be relatively easily steered by curving the entire body in the desired direction. This can be achieved by adding an angular bias to each motion's control, as follows

$$\alpha_i(t) \leftarrow \alpha_i(t) + \alpha_{\text{bias}} \tag{9}$$

where the bias angle $\alpha_{\text{bias}} \in \mathbb{R}$ is positive for a left turn and negative for a right turn. We mapped this value ranging from $-10°$ to $10°$ linearly to the input of one of the analog sticks of our joystick, providing intuitive control when steering the robot.

6. Experiments

We validated our snake robot through a series of indoor experiments. We primarily evaluated the locomotion capabilities of our robot, focusing on validating the effectiveness of global bending and twisting actuation in producing snake locomotion in various directions. The efficiency of the robot's movements was assessed by measuring locomotion velocities. Additionally, we demonstrated the robot's steerability by navigating a 90° corner in an indoor corridor.

Detailed procedures for motion parameter selection and experiment conduction are provided first, followed by the assessment results of the robot's locomotion.

6.1. Motion Parameter Selection

The motion parameters of the motor swing include $\alpha_{\max}$, T, and $\Delta\psi$, as used in (6). Additionally, the locomotion parameters are the pulling displacements of the globally routed tendons. These tendon displacements for vertical upper bending, vertical lower locomotion, and axial twisting are denoted as L_{u}, L_{l}, and L_{t}, respectively. We remark again that the tendons routed through the back of the robot are pulled to create upper bending for forward locomotion, those on the abdomen are pulled to cause lower bending for backward locomotion, and the spiral tendons are pulled for sidewinding. The change in tendon pulling displacements directly affects the resulting locomotion velocities. In general, increasing the magnitude of the tendon pulling parameter that corresponds to a specific gait leads to greater propulsion efficiency in that direction. This relationship can be summarized as follows: 1) Higher L_{u} results in higher forward locomotion velocity. 2) Higher L_{l} results in higher backward locomotion velocity. 3) Higher L_{t} results in higher lateral velocity during sidewinding.

Some of these motion parameters were initially selected based on desired motion properties and subsequently fine-tuned. For example, the amplitude of the motor swing, $\alpha_{\max}$, determines the curving shape of the robot. As we did in our previous work,[17] the robot's initial configuration for each locomotion mode was selected to consist of three curving sections, each making a 180° turn, similar to the configurations in Figure 3–5. With 12 joints in our robot, each curving section comprises four joints. Therefore, $\alpha_{\max}$ was chosen to be $\alpha_{\max} = 90.18°$ for the first four joints to achieve a total bending angle of 180° at $t = 0$ sec. This value was fine-tuned for each motor during experiments. Similarly, the phase shift between motors, $\Delta\psi$, was chosen as $\Delta\psi = 45°$ so that each curving section comprises four motors.

The time period of undulation, T, and the globally routed tendon displacements were determined empirically as given in **Table 1**. These parameters were selected to achieve a balanced trade-off between motion speed and long-term durability, ensuring continuous and stable operation without causing excessive mechanical stress or instability. Additionally, we observed that the head part curves less than the tail part does, likely due to the dynamic effect of the undulatory motion. To compensate for this, we added a small angle to $\alpha_{\max}$ that gradually decreased for 27.5° to 0° from the head to the tail.

6.2. Experimental Procedure

All parameters were set and managed in our desktop application, which was connected to the robot's Arduino board through BLE. A joystick was utilized to control the robot, with a button mapped to planar undulation and an analog stick used to steer the robot left or right. These commands were transmitted to the robot's Arduino board through the desktop application.

Experiments were conducted indoors on a tiled surface, with each tile measuring 30×30 cm. This setup facilitated our observation of the robot's movement and orientation. Upon establishing the BLE connection in each experiment, the robot was initialized in a starting position (i.e., a planar S-shape). The motor motion parameters were applied first, followed by the pulling displacements of the globally routed tendons.

We conducted two experiments to 1) validate the robot's ability to perform different types of snake locomotion and measure the performance, and 2) demonstrate the robot's capability to steer in forward locomotion.

6.3. Locomotion Capability and Performance Assessment

The primary aim of these experiments was to verify if the robot could produce various directional snake movements by actuating the globally routed tendons. As shown in **Figure 11**, our

Table 1. Locomotion parameters.

	Locomotion type		
	Forward	Backward	Sidewinding
Amplitude, $\alpha_{\max}$ [°]		90.18	
Period, T [sec]		3.0	
Phase shift, $\Delta\psi$ [°]		45	
Upper Tendon Pulling, L_{u} [mm]	52.4	–	14.0
Lower Tendon Pulling, L_{l} [mm]	–	69.8	–
Spiral Tendon Pulling, L_{t} [mm]	–	–	27.9

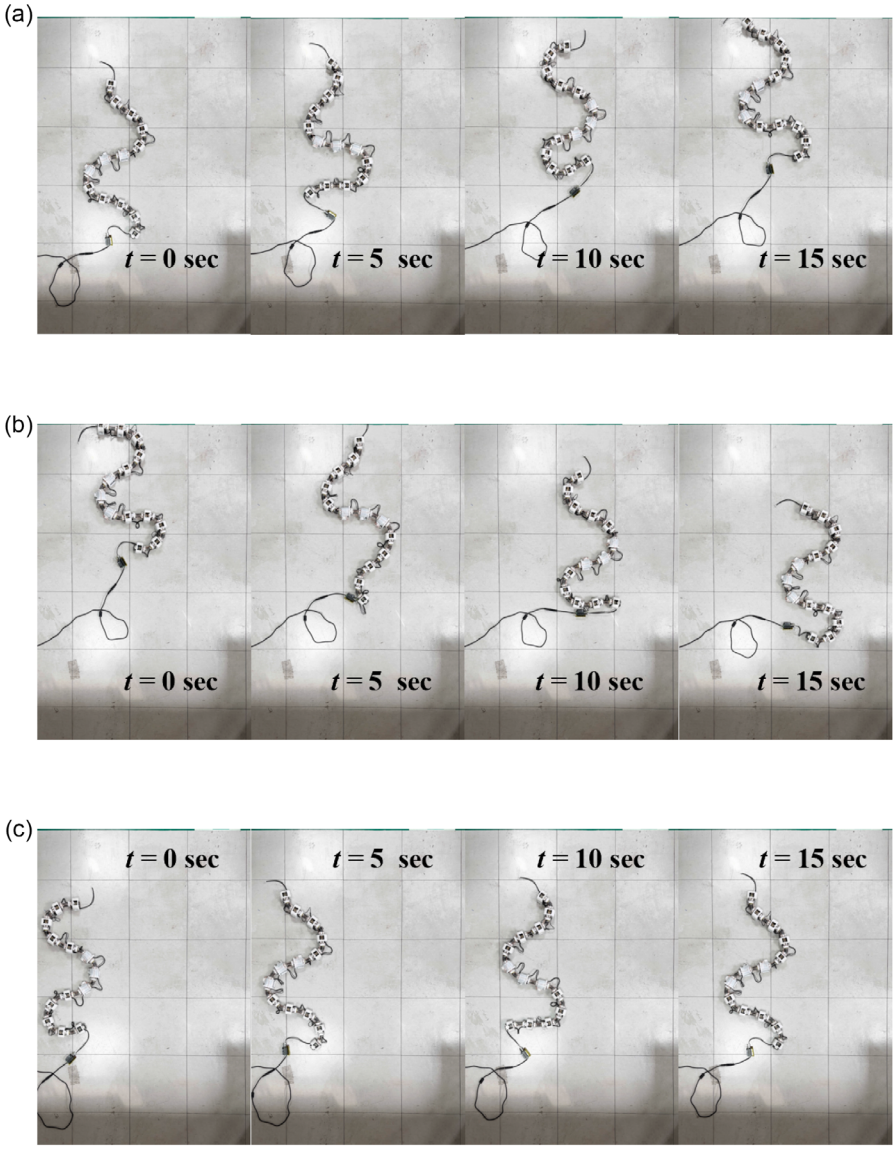

Figure 11. Various types of snake locomotion demonstrated by our robot: a) forward locomotion, b) backward locomotion, and c) sidewinding.

experiments demonstrated the robot's ability to perform various types of locomotion. As expected, pulling the tendons for vertical upper and lower bending made the robot move forward and backward, respectively, and pulling the spiral tendons generated an axial twist, resulting in sidewinding motion. These locomotion results are also included in the first part of the Supplement video (experiment video.mp4).

Beyond demonstrating the locomotion capability, we measured the velocities of these motions as a performance metric. The resulting velocities are given in **Table 2**. The forward, backward, and sidewinding motions achieved speeds of 27.6, 35.5, and 20.0 mm sec^{-1}, respectively

Although the robot demonstrated various locomotion patterns effectively, the achieved speeds were relatively slow. This is attributed to several factors. The tendon-driven mechanism and the use of compliant components, as opposed to rigid ones, introduced complexity and variability in the motion. The primary issue we experienced in the experiments was the robot flipping over, causing signal wires, tendons, and springs to tangle together. The cause of this behavior was identified as torsional backlashes and insufficient torsional stiffness of the continuum joints. Considering that these joints were built by hand using promptly available components in the market, better manufacturing may take a significant amount of time.

Table 2. Performance measurements.

	Locomotion type		
	Forward	Backward	Sidewinding
Speed [mm sec^{-1}]	27.6	35.5	20.0

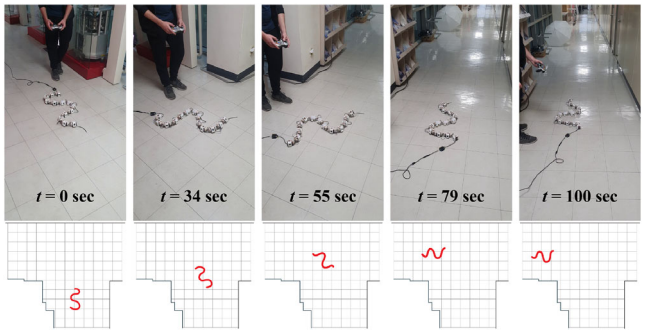

Figure 12. Robot's steerability demonstrated by navigating a 90° corner in an indoor corridor. Each tile block on the floor is 30 × 30 cm.

This behavior was more pronounced when the motion parameters were chosen for faster motion. Increasing the undulation frequency or actuating tendons for more vertical bending and axial twisting led to more instability in the motion.

6.4. Steerability Demonstration

Lastly, we demonstrated the steerability of our robot using joystick inputs. We mapped an analog stick to a continuous steering input that adds a bias angle to the motor positions. We tested our robot by teleoperating it to navigate a 90° corner in an indoor corridor and confirmed that the robot could smoothly turn around the corner. In this particular experiment, the robot required ≈60 sec to complete a 90° turn in the indoor corridor while maintaining alignment along the path. This motion is shown in **Figure 12** and can also be found in the Supplement video (experiment video.mp4).

6.5. Experimental Assessment

The demonstrated locomotion speeds are lower than those of biological snakes and certain rigid snake robots; however, this outcome primarily results from the simplified mechanical design and the intentional focus on validating the locomotion principle rather than optimizing performance. The present prototype functions as a proof-of-concept system, experimentally confirming that distinct locomotion modes can emerge solely from controlled ground-contact configurations and global tendon actuation. While friction anisotropy and stiffness optimization were not emphasized in this version, future improvements—such as minimizing tendon friction, tuning joint compliance, and incorporating optional anisotropic skins—are expected to enhance efficiency and dynamic stability without altering the fundamental actuation and locomotion mechanism.

7. Conclusion

In this article, we presented the development and validation of a tendon-driven compliant snake robot capable of global bending and twisting actuation. Building on our previous theoretical study on snake locomotion principles, we designed a robotic mechanism that emulates the natural ground contact of biological snakes, utilizing body compliance and gravitational deflection. The body compliance was achieved through compliant continuum joints used to concatenate modules. A desktop application with a wireless joystick interface was developed to enable intuitive teleoperation.

Through a series of indoor experiments, we validated the robot's locomotion capabilities, demonstrating effective forward, backward, and sidewinding movements. The measured velocities of these motions were 27.6 mm sec^{-1} for forward, 35.5 mm sec^{-1} for backward, and 20.0 mm sec^{-1} for sidewinding. Moreover, we introduced a method to steer the robot by adding bias angles to the motor control and showcased the robot's steerability by successfully navigating a 90° corner.

The achieved speeds were relatively slow to prevent the robot from flipping over, which was caused by factors such as torsional backlashes and insufficient torsional stiffness of the continuum joints. These issues, primarily attributed to the handmade joints built with readily available components, suggest that improved manufacturing techniques are required to enhance performance. Therefore, our future work will focus on refining the robot's design and control to increase its speed and stability. This includes enhancing the torsional stiffness of the joints and optimizing the locomotion parameters for more efficient locomotion.

This study primarily focused on verifying the feasibility of the proposed global-tension locomotion mechanism rather than demonstrating complex terrain adaptability or optimized performance. The experiments were conducted under controlled indoor conditions to isolate the core actuation principle and validate its effectiveness in generating multiple gaits through ground contacts. The presented system establishes the foundation for subsequent developments that will extend the approach to more diverse environments, improve locomotion efficiency, and enable autonomous transitions through refined mechanical design and control strategies.

Supporting Information

Supporting Information is available from the Wiley Online Library or from the author.

Acknowledgements

S.I. and S.K. contributed equally to this work. This work was supported by the National Research Foundation (NRF) of Korea under the grant no. RS-2022-NR071784 funded by the Korea government (MSIT).

Conflict of Interest

The authors declare no conflict of interest.

Data Availability Statement

Data sharing is not applicable to this article as no new data were created or analyzed in this study.

Keywords

continuum robot, snake robot, snake locomotion, tendon-driven robot

Received: September 23, 2025
Revised: November 5, 2025
Published online:

[1] M. Mori, S. Hirose, in *IEEE/RSJ Inter. Conf. on Intelligent Robots and Systems*, Vol. *1*, IEEE **2002**, pp. 829–834.
[2] T. Kamegawa, T. Harada, A. Gofuku, in *2009 IEEE international conference on robotics and automation*, IEEE **2009**, pp. 3067–3072.
[3] A. Crespi, A. J. Ijspeert, *IEEE Trans. Rob.* **2008**, *24*, 75.
[4] S. A. Fjerdingen, P. Liljebäck, A. A. Transeth, in *2009 IEEE/RSJ Inter. Conf. on Intelligent Robots and Systems*, pp. 5665–5671, IEEE **2009**.
[5] B. Murugendran, A. A. Transeth, S. A. Fjerdingen, in *2009 IEEE/RSJ Inter. Conf. on Intelligent Robots and Systems*, IEEE **2009**, pp. 3643–3650.
[6] A. A. Transeth, R. I. Leine, C. Glocker, K. Y. Pettersen, P. Liljebäck, *IEEE Trans. Rob.* **2008**, *24*, 88.
[7] M. J. Travers, J. Whitman, P. E. Schiebel, D. I. Goldman, H. Choset, *Rob.: Sci. Syst.* **2016**, *12*.
[8] P. Liljeback, K. Y. Pettersen, Ø. Stavdahl, J. T. Gravdahl, *IEEE/ASME Trans. Mechatron.* **2011**, *17*, 1158.
[9] P. Liljeback, K. Y. Pettersen, Ø. Stavdahl, J. T. Gravdahl, *IEEE Trans. Rob.* **2011**, *27*, 792.
[10] C. Wright, A. Johnson, A. Peck, Z. McCord, A. Naaktgeboren, P. Gianfortoni, M. Gonzalez-Rivero, R. Hatton, H. Choset, in *2007 IEEE/RSJ Inter. Conf. on Intelligent Robots and Systems*, IEEE **2007**, pp. 2609–2614.
[11] C. Wright, A. Buchan, B. Brown, J. Geist, M. Schwerin, D. Rollinson, M. Tesch, H. Choset, in *2012 IEEE Inter. Conf. on Robotics and Automation*, IEEE **2012**, pp. 4347–4354.
[12] D. Rollinson, H. Choset, *J. Field Rob.* **2016**, *33*, 322.
[13] H. Marvi, C. Gong, N. Gravish, H. Astley, M. Travers, R. L. Hatton, J. R. Mendelson, H. Choset, D. L. Hu, D. I. Goldman, *Science* **2014**, *346*, 224.
[14] M. Luo, M. Agheli, C. D. Onal, *Soft Rob.* **2014**, *1*, 136.
[15] C. Branyan, C. Fleming, J. Remaley, A. Kothari, K. Tumer, R. L. Hatton, Y. Mengüç, in *2017 IEEE Inter. Conf. on Robotics and Biomimetics (ROBIO)*, IEEE **2017**, pp. 282–289.
[16] B. Liao, H. Zang, M. Chen, Y. Wang, X. Lang, N. Zhu, Z. Yang, Y. Yi, *Soft Rob.* **2020**, *7*, 500.
[17] J. Ha, *IEEE Trans. Rob.* **2023**, *39*, 3875.
[18] G. Mengaldo, F. Renda, S. L. Brunton, M. Bächer, M. Calisti, C. Duriez, G. S. Chirikjian, C. Laschi, *Nat. Rev. Phys.* **2022**, *4*, 595.
[19] D. L. Hu, J. Nirody, T. Scott, M. J. Shelley, *Proc. Natl. Acad. Sci.* **2009**, *106*, 10081.
[20] S. Yu, S. Ma, B. Li, Y. Wang, in *2009 Inter. Conf. on Information and Automation*, IEEE **2009**, pp. 500–505.
[21] K. Togawa, M. Mori, S. Hirose, in *Proc. 2000 IEEE/RSJ Inter. Conf. on Intelligent Robots and Systems (IROS 2000)(Cat. No. 0°CH37113)*, Vol. *3*, IEEE **2000**, pp. 2242–2247.
[22] D. Rollinson, K. V. Alwala, N. Zevallos, H. Choset, in *2014 IEEE/RSJ Inter. Conf. on Intelligent Robots and Systems*, IEEE **2014**, pp. 1093–1099.
[23] W. Wei, J. X. Yu, W. H. Lin, R. S. Mai, C. X. Chen, Z. Y. He, Z. Li, *Appl. Mech. Mater.* **2014**, *598*, 610.
[24] W. Xiao, Y. Gao, W. Wei, J. Zhang, X. Tan, *J. Phys.: Conf. Series* **2021**, *1754*, 012152, IOP Publishing.
[25] T. Takemori, M. Tanaka, F. Matsuno, in *2018 IEEE/RSJ Inter. Conf. on Intelligent Robots and Systems (IROS)*, IEEE **2018**, pp. 1–9.
[26] T. Takemori, M. Tanaka, F. Matsuno, *IEEE Trans. Rob.* **2021**, *37*, 1696.
[27] F. Trebuňa, I. Virgala, M. Pástor, T. Lipták, L. Miková, *Int. J. Adv. Rob. Syst.* **2016**, *13*, 1729881416663668.
[28] Y. Bando, H. Suhara, M. Tanaka, T. Kamegawa, K. Itoyama, K. Yoshii, F. Matsuno, H. G. Okuno, in *2016 IEEE Inter. Symp. on Safety, Security, and Rescue Robotics (SSRR)*, IEEE **2016**, pp. 207–213.
[29] C. Branyan, R. L. Hatton, Y. Mengüç, *IEEE Rob. Autom. Lett.* **2020**, *5*, 1728.
[30] D. D. Arachchige, D. M. Perera, S. Mallikarachchi, I. Kanj, Y. Chen, I. S. Godage, in *2023 IEEE Inter. Conf. on Soft Robotics (RoboSoft)*, IEEE **2023**, pp. 1–6.
[31] F. Rozaidi, E. Waters, O. Dawes, J. Yang, J. R. Davidson, R. L. Hatton, in *2023 IEEE Inter. Conf. on Soft Robotics (RoboSoft)*, IEEE **2023**, pp. 1–7.
[32] T. Kano, A. Ishiguro, *Integr. Comp. Biol.* **2020**, *60*, 232.
[33] H. C. Astley, C. Gong, J. Dai, M. Travers, M. M. Serrano, P. A. Vela, H. Choset, J. R. Mendelson, D. L. Hu, D. I. Goldman, *Proc. Natl. Acad. Sci.* **2015**, *112*, 6200.
[34] A. A. Transeth, R. I. Leine, C. Glocker, K. Y. Pettersen, *IEEE Trans. Rob.* **2008**, *24*, 361.
[35] J. Koley, D. Sharma, D. Chakraborty, H. K. Pillai, in *2025 IEEE Inter. Conf. on Robotics and Automation (ICRA)* **2025**, pp. 12296–12302.
[36] A. Parvaresh, B. Seyidoğlu, A. Rafsanjani, in *2024 IEEE 7th Inter. Conf. on Soft Robotics (RoboSoft)* **2024**, pp. 519–524.
[37] S. Manzoor, U. Khan, I. Ullah, *Iran. J. Sci. Technol., Trans. Electr. Eng.* **2020**, *44*, 1093.
[38] S. Manzoor, Y. G. Cho, Y. Choi, *J. Intell. Rob. Syst.* **2019**, *94*, 641.
[39] R. J. Webster III, B. A. Jones, *Int. J. Rob. Res.* **2010**, *29*, 1661.